

# A Novel Nonenzymatic Hydrogen Peroxide Electrochemical Sensor Based on Facile Synthesis of Copper Oxide Nanoparticles Dopping into Graphene Sheets@Cerium Oxide Nanocomposites Sensitized Screen Printed Electrode

Guo-wen He<sup>1</sup>, Jian-qing Jiang<sup>2,\*</sup>, Dan Wu<sup>1</sup>, Yi-lan You<sup>1</sup>, Xin Yang<sup>3,4,\*</sup>, Feng Wu<sup>3,4</sup>, Yang-jian Hu<sup>3,4</sup>

<sup>1</sup> College of Chemical and Environmental Engineering, Hunan City University, Yiyang, 413000, P.R. China;

<sup>2</sup> School of Civil Engineering, Hunan City University, Yiyang, 413000, P.R. China;

<sup>3</sup> Huaihua Key Laboratory of Functional Inorganic&Polymeric Materials, College of Chemistry and Materials Engineering, Huaihua University, Huaihua 418000, P.R. China;

<sup>4</sup> Key Laboratory of Rare Earth Optoelectronic Materials&Devices, College of Chemistry and Materials Engineering, Huaihua University, Huaihua 418000, P.R. China;

\*E-mail: [zhongyipp@163.com](mailto:zhongyipp@163.com); [01yangxin@163.com](mailto:01yangxin@163.com)

Received: 23 April 2016 / Accepted: 8 August 2016 / Published: 6 September 2016

---

A novel electrochemical sensor for nonenzymatic hydrogen peroxide (H<sub>2</sub>O<sub>2</sub>) detecting based on facile synthesis of copper oxide (CuO) nanoparticles dopping into graphene sheets@cerium oxide nanocomposites sensitized screen printed electrode (SPE) was fabricated. CuO nanoparticles were dopped into GS@CeO<sub>2</sub> nanocomposites via a facile solvothermal process. X-ray powder diffractometer (XRD) combines with fourier transform infrared spectroscopy (FTIR) were used to characterize the composition of GS@CeO<sub>2</sub>-CuO nanocomposites. Electrochemical impedance spectroscopy (EIS) was utilized to study the interfacial properties as well as scanning electron microscopy (SEM) was employed to characterize the morphologies of different electrodes. The electrochemical properties of electrochemical sensor were investigated by cyclic voltammetry (CV) and chronoamperometry (i-t curve) methods. After all experimental parameters were optimized, the GS@CeO<sub>2</sub>-CuO hybrid nanomaterials modified SPE (SPE | GS@CeO<sub>2</sub>-CuO) showed a good performance towards the electrocatalytic reduction of H<sub>2</sub>O<sub>2</sub>. A wide linear detection range (LDR) of CV peaks from 5.0×10<sup>-3</sup> mM to 18.0 mM (*R*=0.9994) and a low limit of detection (LOD) of 2.1×10<sup>-3</sup> mM (*S/N*=3) was achieved. The proposed electrochemical sensor was quick, selective, sensitive, simple, stable and reliable to quantitative determination of trace H<sub>2</sub>O<sub>2</sub> in real samples.

---

**Keywords:** Copper oxide; Graphene sheets@cerium oxide; Screen printed electrode; Nonenzymatic; Hydrogen peroxide.

## 1. INTRODUCTION

Hydrogen peroxide ( $H_2O_2$ ) is a necessary analytical object during some chemical, clinical, biological, pharmaceutical, environmental and food analysis processes, and also an important by-product of many oxidase enzymes. Therefore, exploring the selective, sensitive, simple, quick, stable and reliable analytical techniques and methods for quantitative determination of  $H_2O_2$  have attracted much attention [1-3].

Many analytical techniques and methods, such as electrochemistry techniques [4-7], chromatography [8, 9], chemiluminescence [10] and titrimetry [11] have been developed to monitor the concentration of  $H_2O_2$ . Compared with the other techniques, the enzyme-involved electrochemical biosensors are widely used attribute to their selectivity, sensitivity, portability and fast response. Horseradish peroxidase (HRP) [12], hemoglobin (Hb) [13], myoglobin (Mb) [14, 15] and cytochrome c (Cyt c) [16] contain iron centered porphyrin and can easily undergo the redox reactions, thus catalyzing the electrochemical oxidation or reduction of  $H_2O_2$ . Those enzymes are commonly utilized to fabricate enzyme-involved  $H_2O_2$  electrochemical biosensors. However, those enzyme-modified electrodes often suffered from some disadvantages. Firstly, those enzymes are usually expensive and cause the high cost of the modified electrodes. Secondly, the complicated immobilization procedures of enzymes result in tedious and time-consuming modifying steps. Moreover, experimental conditions or toxic chemicals might be seriously affected the activity of enzymes and induce great difficulties for the assembly, storage and use of enzyme-involved biosensors [17-19].

With the aim of overcoming these problems, massive studies have been made on the materials with outstanding properties for nonenzymatic  $H_2O_2$  electrochemical sensors, such as carbon materials [20, 21], noble metals nanoparticles [22, 23], metal alloys [24, 25] and metal oxides [26-28]. Although all the mentioned materials show nice signals and performances, the development of novel nanocomposites with high sensitive and selective catalyst for nonenzymatic  $H_2O_2$  detection is still in great demand. Compared with single component, the nanocomposites have certain synergistic effects. For example, nice signal-to-noise ratio, fast electron transport and larger surface area, et al.

To date, graphene sheets (GS) integrated with other nanomaterials have been considered as the advanced composite materials in fabricating  $H_2O_2$  sensors [29-31]. Owing to the vast surface-to-bulk ratio, low toxicity, high electronic conductivity, excellent biocompatibility and good chemical stability, cerium dioxide nanostructure ( $CeO_2$ ) has also been widely investigated as a promising semiconductor oxide material for electrochemical sensors, including nonenzymatic  $H_2O_2$  detection [32, 33]. Copper oxide (CuO) nanoparticles have massive available active sites as well as large electrochemically active surface area toward the electrochemical reaction of  $H_2O_2$ . Thus, resulting in a high-performance amperometric response of  $H_2O_2$  molecules detection [34-38]. Given that, we reasonable to expect that GS,  $CeO_2$  and CuO hybrid nanomaterials would provide a nice electrochemical activity with the amperometric sensing of  $H_2O_2$ .

Although many literature has been released on the decorating of CuO on GS or reduced graphene oxide (rGO)[39, 40], so far as we know, no attention has been paid to prepare of CuO doping into GS@ $CeO_2$  nanocomposites modified electrode for nonenzymatic  $H_2O_2$  detection.

Actually, the catalytic activity to  $\text{H}_2\text{O}_2$  detection is greatly effected by the respective particles and synergistic effects of hybrid nanomaterials.

The aim of this paper is to fabricate a selective and sensitive nonenzymatic  $\text{H}_2\text{O}_2$  electrochemical sensor based on CuO doping into GS@ $\text{CeO}_2$  nanocomposites modified screen printed electrode (SPE) for the first time. The proposed SPE | GS@ $\text{CeO}_2$ -CuO electrode shows significantly enhanced respond currents and superior electrochemical activity for  $\text{H}_2\text{O}_2$  determination due to the good synergistic effects. Meanwhile, the SPE | GS@ $\text{CeO}_2$ -CuO electrode exhibits obviously improved selectivity attributed to its low reduction working potential (-0.5 V vs Ag/AgCl). Finally, the electrochemical sensor is applied to analyze  $\text{H}_2\text{O}_2$  in real samples with nice accuracy and recovery.

## 2. EXPERIMENTAL

### 2.1. Reagents and apparatus

Graphite powder, nafion (Nf) solution, 30%  $\text{H}_2\text{O}_2$  solution,  $\text{Cu}(\text{NO}_3)_2 \cdot 3\text{H}_2\text{O}$  and all other chemicals with analytical grade were purchased from Sinopharm Medicine Holding Co., Ltd (Shanghai, China).  $\text{CeCl}_3 \cdot 7\text{H}_2\text{O}$  was obtained from Tianjin Guangfu Fine Chemical Research Institute (Tianjin, China). The stock solutions of 0.1 M  $\text{NaH}_2\text{PO}_4$  and 0.1 M  $\text{Na}_2\text{HPO}_4$  with various proportion were mixed to prepare different pH values of 0.1 M phosphate buffer solution (PBS). Contact lens care solution was obtained nearby Hunan City University (2016.2). All experiments were performed under  $\text{N}_2$  protection and doubly distilled water with 18.2 M $\Omega$  resistance was used throughout.

The morphologies of bare and modified SPEs were characterized with scanning electron microscopy (SEM, Zeiss Sigma HD). The fourier transform infrared spectroscopy (FTIR) of the nanomaterials with the KBr pellet were recorded on a IR prestige-21 spectrometer (Shimadzu). The crystallization degree or phase purity of the samples were determined by x-ray powder diffractometer (XRD, Cu K $\alpha$  radiation, Rigaku Ultima IV). All electrochemical measurements were carried out on the SPEs, which connected to an electrochemical workstation (CHI 660D, Chenhua Instruments). The SPEs integrated with three electrodes were purchased from DropSens corporation (Spain, the working electrode was carbon or modified, the auxiliary and reference electrodes were carbon and Ag/AgCl electrodes, respectively.).

### 2.2. Synthesis of GS@ $\text{CeO}_2$ -CuO nanocomposites

In a typical experiment, the GS@ $\text{CeO}_2$ -CuO nanocomposites were prepared via a facile solvothermal process. In the first step, a modified Hummers method was employed to synthesize graphene oxide (GO) from graphite powder [12]. Then, 40.0 mg of  $\text{CeCl}_3 \cdot 7\text{H}_2\text{O}$ , 0.20 mL of propylene oxide and 20.0 mL of 1.0 mg/mL GO aqueous solution were added into 10.0 mL of DMF under magnetic stirring. During this process, the GO's functionalities react with  $\text{Ce}^{3+}$  and the addition of propylene oxide drives the formation of GS@ $\text{CeO}_2$ . Finally, 25.0 mg of  $\text{Cu}(\text{NO}_3)_2 \cdot 3\text{H}_2\text{O}$  used as the source of CuO and 0.1 mL of 2.0 M NaOH solution were added into the above dispersions. The

mixture was sealed into a 50 mL Teflon-lined stainless steel autoclave and kept at 100 °C for 4 hours. After that, the autoclave was placed in air and allowed to cool. The resulting stable black dispersion was centrifuged and thoroughly washed with doubly distilled water. The final product was denoted as GS@CeO<sub>2</sub>-CuO. As a comparison, GS@CeO<sub>2</sub> was synthesized in the same way as the GS@CeO<sub>2</sub>-CuO nanocomposites.

### 2.3. Preparation of the modified electrode

A total of 5.0 mg obtained GS@CeO<sub>2</sub>-CuO nanocomposites was redispersed into 1.0 mL of Nf solution (wt%=0.5%) by 10 min of vigorous ultrasonication to achieve homogeneous suspension. Then the resulting suspension of 10.0 μL was dropped onto the surface of SPE and left to get dried at room temperature (labeled as SPE | GS@CeO<sub>2</sub>-CuO). In the control experiments, the GS and GS@CeO<sub>2</sub> modified electrode were fabricated by GS solution (5.0 mg/mL) and GS@CeO<sub>2</sub> solution (5.0 mg/mL) depositing onto other SPEs, respectively (labeled as SPE | GS and SPE | GS@CeO<sub>2</sub>).

### 2.4. Analytical procedures

The SPE | GS@CeO<sub>2</sub>-CuO electrode was immersed into a beaker containing 2.0 mL of pH=7.0 PBS and then N<sub>2</sub> was purged for 15 min. After that, different concentration of H<sub>2</sub>O<sub>2</sub> standard solutions were successively added into PBS. Cyclic voltammogram (CV) was employed to study the nonenzymatic detection and quantitative analyze of H<sub>2</sub>O<sub>2</sub>. The CV measurements with a scan rate of 0.1 V/s was carried out from -1.0 V to +0.4 V. The chronoamperometry (i-t curve) measurements were used to investigate the selectivity and the working potential was -0.5 V. The schematic diagram of the surface of working electrode and possible reduction mechanism of H<sub>2</sub>O<sub>2</sub> were shown in Fig.1. N<sub>2</sub> protection were carried out throughout. The contact lens care solutions were diluted and used directly, and the recommended procedures as mentioned above were followed. To confirm the accuracy of this method, the conventional KMnO<sub>4</sub> titration method was compared with the obtained results.

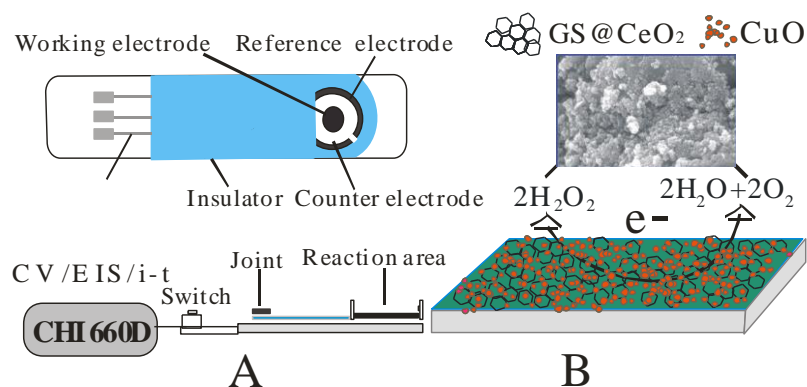


**Figure 1.** The schematic diagram of the electrochemical sensor apparatus (A) and possible reduction mechanism of H<sub>2</sub>O<sub>2</sub> (B).

### 3. RESULTS AND DISCUSSION

#### 3.1. Characterization of GS@CeO<sub>2</sub>-CuO nanocomposites

As to GO, the diffraction peak (002) of GO locates at  $2\theta=10.6^\circ$ , which can be explained by the introduction of numerous epoxy, carboxyl, hydroxyl and carbonyl oxygenic functional groups (Fig.2a) [12]. The XRD of GS is displayed in Fig.2b. The poor diffraction peak is in good agreement with graphite at around  $2\theta=23^\circ$ . That is ascribed to the various oxygen-containing functional groups partial disappeared during the reduction process and restacked into a disordered crystalline structure [41]. It is obvious that there is almost complete reduction of GO by the disappearance of the characteristic peak at  $10.6^\circ$  and all other peaks of GS@CeO<sub>2</sub> nanocomposites can be indexed to CeO<sub>2</sub> at  $28.6^\circ$  (111),  $33.2^\circ$  (200),  $47.3^\circ$  (220) and  $56.2^\circ$  (222) in GS@CeO<sub>2</sub> nanocomposites according to the good agreement with JCPDS card (no. 81-0792) [32] (Fig.2c). After CuO decorated on GS@CeO<sub>2</sub> nanocomposites, the XRD pattern of GS@CeO<sub>2</sub>-CuO nanocomposites (Fig.2d) shows seven additional peaks at  $32.5^\circ$  (110),  $38.7^\circ$  (111),  $48.7^\circ$  (202),  $53.5^\circ$  (020),  $58.4^\circ$  (202),  $61.6^\circ$  (113) and  $68.2^\circ$  (220) match with the standard monoclinic cubic structure of CuO (JCPDS card no.80-1298) [39].

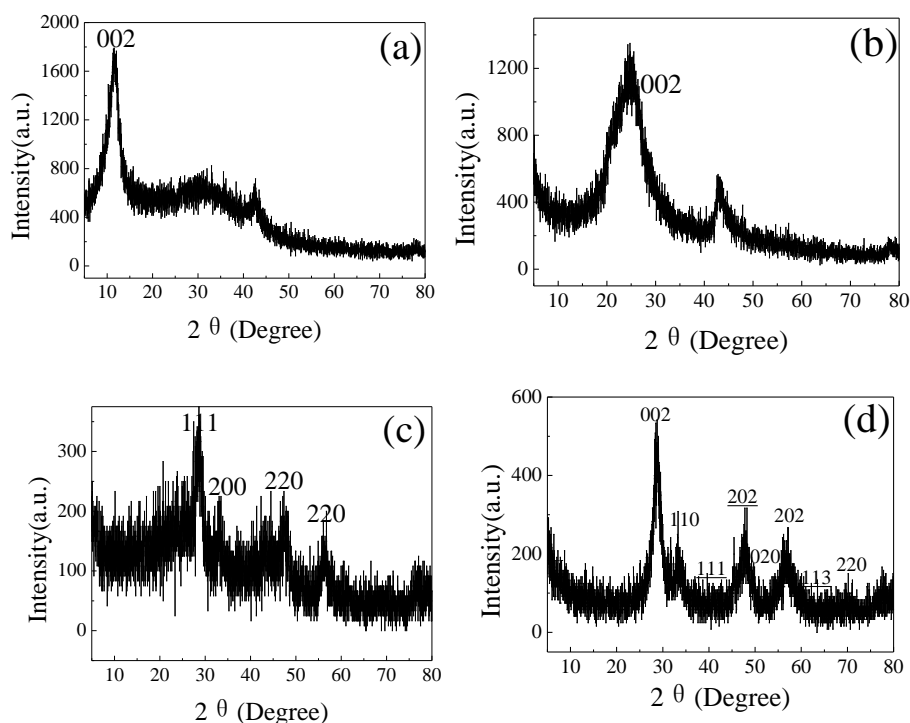


**Figure 2.** XRD patterns of GO (a), GS (b), GS@CeO<sub>2</sub> (c) and GS@CeO<sub>2</sub>-CuO nanocomposites (d).

The FTIRs of GO, GS, GS@CeO<sub>2</sub> and GS@CeO<sub>2</sub>-CuO nanocomposites are illustrated in Fig. 3. In the FTIR of GO (Fig.3a), stretches of aromatic C=C, C=O, O-H, alkoxy, carboxyl C-O and epoxy C-O could be found at 1620, 1730, 3400, 1060, 1410 and 1230 cm<sup>-1</sup>, respectively, in good consistent with previous paper [24]. In contrast, some of the oxygen function groups' peaks are obviously weakened or entirely disappeared in the FTIR of GS (Fig. 3b). The FTIR of GS@CeO<sub>2</sub> nanocomposite

(Fig. 3c) displays peaks at 1620 and 1410  $\text{cm}^{-1}$  could attribute to the skeletal vibration of the GS and carboxyl C-O. In addition, one absorption band associated with the coupling mode between Ce-O stretching modes in the face-centered cubic structure could be found at about 950  $\text{cm}^{-1}$ . Moreover, There is no obvious changes in the FTIR of GS@CeO<sub>2</sub>-CuO nanocomposite (Fig. 3d) compared with GS@CeO<sub>2</sub> nanocomposite. Thus, the formation of GS@CeO<sub>2</sub>-CuO nanocomposites was further confirmed by FTIRs.

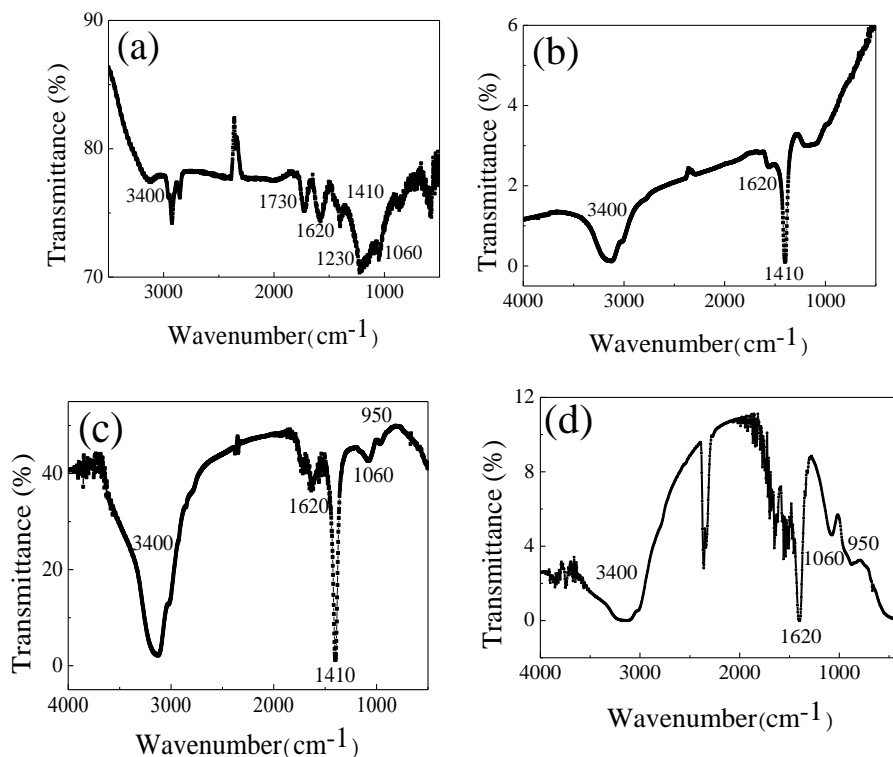


**Figure 3.** FTIRs of GO (a), GS (b), GS@CeO<sub>2</sub> (c) and GS@CeO<sub>2</sub>-CuO nanocomposites (d).

### 3.2. Characterization of different electrodes' surface

The SPE appears the flake graphite on its surface (Fig.4a) [42]. Some thin wrinkles on the surface of SPE | GS electrode are observed in the magnified SEM image, confirming the layered structure of GS (Fig.4b) [42]. When the GS@CeO<sub>2</sub> nanocomposites are dropped onto the surface of SPE to fabricate the SPE | GS@CeO<sub>2</sub> electrode, uniform GS@CeO<sub>2</sub> nanocomposites form randomly on the SPE with about 20 nm to 30 nm in average diameter (Fig.4c) [43]. The SEM micrograph also shows that CuO are uniformly doped into the surface of GS@CeO<sub>2</sub> nanocomposites (Fig.4d). The particle sizes of CuO calculated from SEM images are found to be 10 nm. Obviously, the CuO could be homogeneously doped into the GS@CeO<sub>2</sub> matrix. Energy dispersive spectrometer (EDS) was used to identify the chemical composition of the GS@CeO<sub>2</sub>-CuO nanocomposites in the marked points in SEM image of GE | GS@CeO<sub>2</sub>-CuO electrode (Fig.4e), which confirms the presence of C, O, Ce and Cu elements.

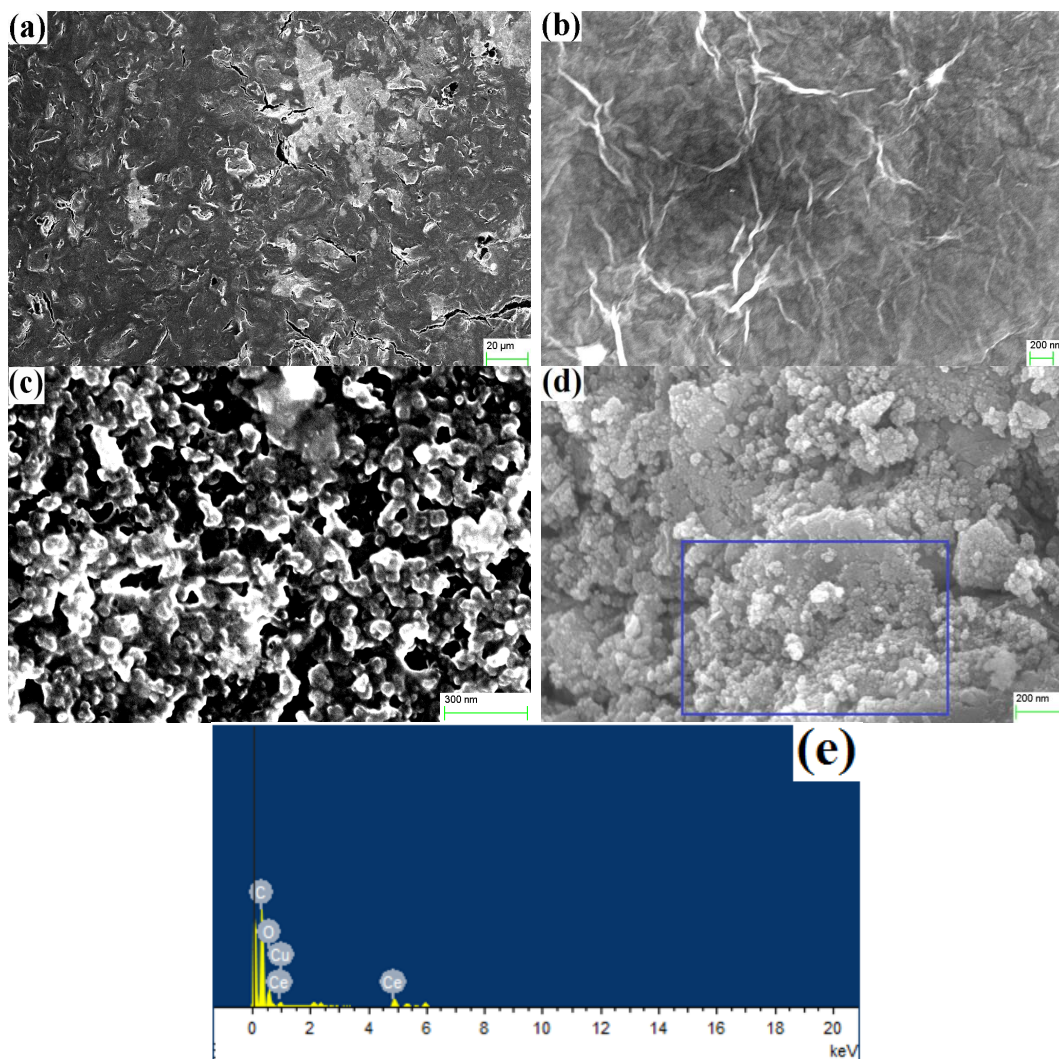


**Figure 4.** SEM images of SPE (a), SPE | GS (b), SPE | GS@CeO<sub>2</sub> (c) and SPE | GS@CeO<sub>2</sub>-CuO (d) electrodes and EDS of marked points in SEM image of SPE | GS@CeO<sub>2</sub>-CuO electrode (e).

### 3.3. Electrochemical behaviors of different electrodes

The electrochemical impedance spectroscopy (EIS) is used to investigate the interfacial properties of different electrodes, shown in Fig.5. Generally, the Nyquist plots shows the imaginary part ( $-Z''$ ) and real part ( $Z'$ ) on the Y-axis and X-axis, respectively. The spectrum includes a linear part and a semicircle part, of which the linear part at low frequencies and semicircle part at high frequencies correspond to the diffusion process and electron transfer limited process, respectively. The diameter of the semicircle part equals to the charge transfer resistance ( $R_{ct}$ ). The SPE's EIS shows a very small semicircle diameter with a negligible  $R_{ct}$  value (Fig.5a), implying that the characteristic of a diffusional limiting step of the  $[\text{Fe}(\text{CN})_6]^{3-/4-}$  electrochemical process. When the SPE is modified with GS, the semicircle's diameter increases a little (Fig. 5b), which is ascribed to the fact that Nf used to fix nanomaterials would block the diffusion of  $[\text{Fe}(\text{CN})_6]^{3-/4-}$  although GS has high electrical conductivity [44]. The diameter of the semicircle of SPE | GS@CeO<sub>2</sub> electrode (Fig.5c) increases dramatically compared with the SPE | GS electrode. That means the electrochemical activity of

SPE | GS@CeO<sub>2</sub> is lower than SPE | GS, owing to the insulation of CeO<sub>2</sub>. As compared with curve 5c, after CuO doping into the GS@CeO<sub>2</sub> nanocomposites (Fig.5d), the semicircle diameter decreases remarkably, leading to the obvious reduction of R<sub>ct</sub> value. Which is attributed to the CuO could accelerate the electron transfer in the hybrid nanomaterials.

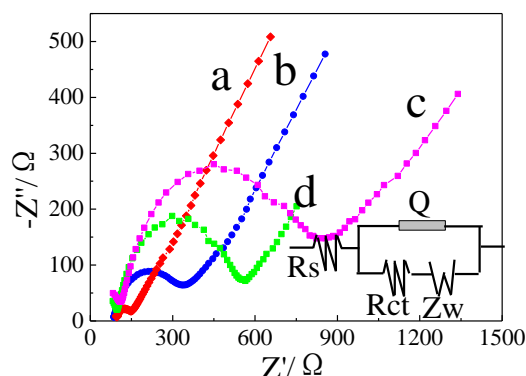


**Figure 5.** EIS of SPE (a), SPE | GS (b), SPE | GS@CeO<sub>2</sub> (c) and SPE | GS@CeO<sub>2</sub>-CuO (d) electrodes in 0.1 M KCl solution containing 10 mM [Fe(CN)<sub>6</sub>]<sup>3-/4-</sup> (1:1).

Fig.6 shows the CVs of 5.0 mM H<sub>2</sub>O<sub>2</sub> on different electrodes in 0.1 M PBS (pH=7.0). There is no reduction peak current of H<sub>2</sub>O<sub>2</sub> on the SPE (Fig.6 a) and SPE | GS (Fig.6 b) electrodes. In contrast, obvious reduction peak current at about -0.76 V are found both on the SPE | GS@CeO<sub>2</sub> (Fig.6 c) and SPE | GS@CeO<sub>2</sub>-CuO (Fig.6 d) electrodes, which could be attributed to the reduction of H<sub>2</sub>O<sub>2</sub>.

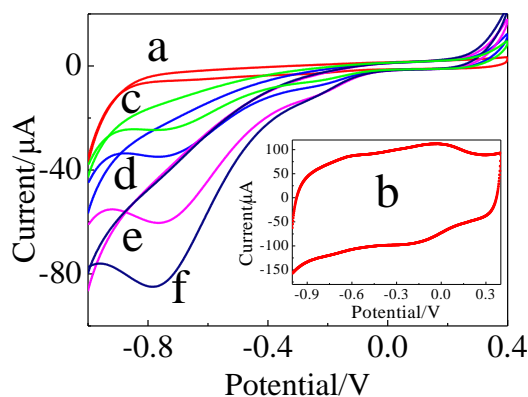


**Figure 6.** CVs of SPE (a), SPE | GS (b), SPE | GS@CeO<sub>2</sub> (c), SPE | GS@CeO<sub>2</sub>-CuO (d) electrodes in presence of 5.0 mM H<sub>2</sub>O<sub>2</sub>, and (d) electrode added with 8.0 (e) and 12.0 mM H<sub>2</sub>O<sub>2</sub> (f).

However, we could not find these peaks in the absence of H<sub>2</sub>O<sub>2</sub> with all proposed electrodes. Furthermore, it is obvious that the SPE | GS@CeO<sub>2</sub>-CuO (Fig.6 d) electrode exhibits higher reduction peak current compared with SPE | GS@CeO<sub>2</sub> (Fig.6 c) electrode. This indicates that GS@CeO<sub>2</sub>-CuO hybrid nanomaterials have stronger activity towards the electrocatalytic reduction of H<sub>2</sub>O<sub>2</sub>. It may be

due to the good electron-transfer ability of GS@CeO<sub>2</sub>-CuO hybrid nanomaterials, forming high electron conduction paths between the electroactive indicator and electrode. The experiments imply that the presence of catalytic property as well as synergistic effect of the GS@CeO<sub>2</sub>-CuO hybrid nanomaterials. Moreover, it is noticeable that the reduction peak current at the SPE | GS@CeO<sub>2</sub>-CuO electrode increases with the increment of H<sub>2</sub>O<sub>2</sub> concentration (Fig.6 e, Fig.6 f). All above reveal the potential application of SPE | GS@CeO<sub>2</sub>-CuO electrode in H<sub>2</sub>O<sub>2</sub> analysis.

### 3.4. Optimization of experimental conditions

The amount of GS@CeO<sub>2</sub>-CuO solution modified to the electrode is one of important parameters for detecting of H<sub>2</sub>O<sub>2</sub>. By dropping different volume of GS@CeO<sub>2</sub>-CuO solution onto SPE, several SPE | GS@CeO<sub>2</sub>-CuO electrodes were fabricated. At first up to 10.0  $\mu$ L, the current responses to 5.0 mM H<sub>2</sub>O<sub>2</sub> increased. The broaden voltammograms with decreased peak currents were observed when higher amount of GS@CeO<sub>2</sub>-CuO solution used. Thus, 10.0  $\mu$ L of GS@CeO<sub>2</sub>-CuO solution is suitable.

The stripping peak currents of SPE | GS@CeO<sub>2</sub>-CuO electrode in various electrolytes, such as 0.1 M PBS, NH<sub>3</sub>·H<sub>2</sub>O-NH<sub>4</sub>Cl, and NaAc-HAc solutions toward 5.0 mM H<sub>2</sub>O<sub>2</sub> were investigated. The biggest stripping peak currents with good shapes and low backgrounds were obtained in PBS. The peak current increased gradually as the pH from 5.5 to 7.0 and then decreased at the higher pHs. Hence, 0.1 M pH=7.0 PBS is employed as the supporting electrolyte, which in agreement with the previous reports [45, 46].

The sensitivity of electrochemical sensor is also greatly influenced by the detection potential. Fig. 7 shows the current responses evaluated at -0.3 V, -0.4 V, -0.5 V and -0.6 V upon the successive addition of 1.0 mM H<sub>2</sub>O<sub>2</sub>. As presented in Fig. 7, the sensitivity gradually decreased from -0.3 V, -0.4 V to -0.5 V. Compared with the potential of -0.6 V, potential of -0.5 V has slight higher response, better stable, and lower background noise. Considering the results above, -0.5 V is chosen.

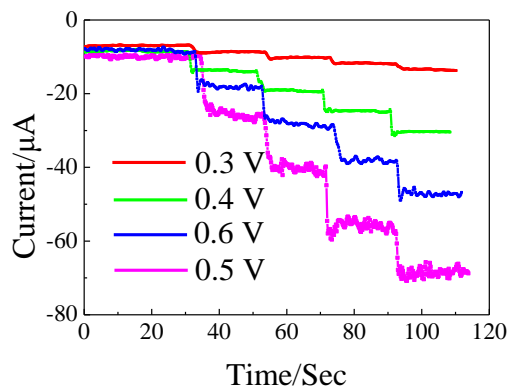


**Figure 7.** i-t responses of the SPE | GS@CeO<sub>2</sub>-CuO electrode upon the successive addition of 1.0 mM H<sub>2</sub>O<sub>2</sub> at different detection potentials.

3.5. Amperometric responses of  $H_2O_2$  on SPE | GS@CeO<sub>2</sub>-CuO electrode

As all the experimental conditions are optimized, the typical CV curves of SPE | GS@CeO<sub>2</sub>-CuO electrode with successive injection of H<sub>2</sub>O<sub>2</sub> are given in Fig. 8. It is obvious that the reduction current increases with increased concentrations of H<sub>2</sub>O<sub>2</sub>. The CVs responses have a good linear relationship to H<sub>2</sub>O<sub>2</sub> in a wide linear detection range (LDR) from  $5.0 \times 10^{-3}$  mM to 18.0 mM with the linearization equation  $i_p = 1.0827 + 5.7192 \times C_{H_2O_2}$  ( $C$ :mM,  $R=0.9994$ ). However, when the H<sub>2</sub>O<sub>2</sub> concentration higher than 18.0 mM, the sensitivity drops because the available electroactive sites and electrode surface area for electrochemical reactions of H<sub>2</sub>O<sub>2</sub> to take place are limited. Based on the signal-noise ratio equals to 3 ( $S/N=3$ ), a low limit of detection (LOD) was estimated to be  $2.1 \times 10^{-3}$  mM.

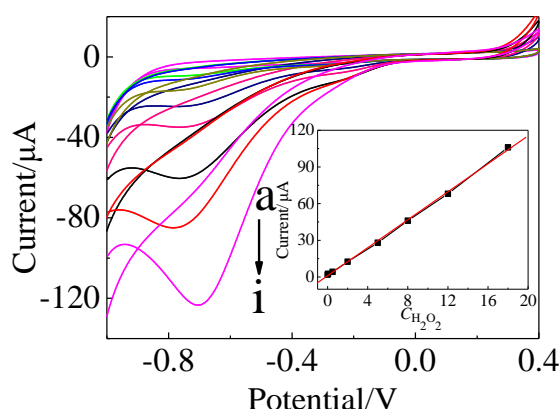


**Figure 8.** CVs of SPE | GS@CeO<sub>2</sub>-CuO electrode for addition different concentration of H<sub>2</sub>O<sub>2</sub> in 0.1 mM PBS. (a) 0, (b) 0.005, (c) 0.05, (d) 0.5, (e) 2.0, (f) 5.0, (g) 8.0, (h) 12.0, (i) 18.0 mM. Inset: calibration curve between current vs  $C_{H_2O_2}$ .

As summarized in Table 1, compared with some other enzymatic or nonenzymatic H<sub>2</sub>O<sub>2</sub> sensors reported previously, the proposed one presents a superior analytical performance. Firstly, the proposed modified electrode could be prepared via a simple, quick and easy procedure. Secondly, it shows a wide LDR as well as a low LOD. Hence, the SPE | GS@CeO<sub>2</sub>-CuO electrode is suitable for the fabrication of a novel nonenzymatic H<sub>2</sub>O<sub>2</sub> electrochemical sensor.

**Table 1.** Comparison of several typical nonenzymatic and enzymatic H<sub>2</sub>O<sub>2</sub> sensors.

Electrode	Linear range/mM	LOD <sup>a</sup> /µM	Ref.
GCE <sup>b</sup>   Au-GS	0.03-5.0	10	[6]
SPE   GS-Nf/Fe <sub>3</sub> O <sub>4</sub> -Au-HRP	0.02-2.5	12	[12]
GCE   Pt/poly-melamine	0.005-1.65	0.65	[23]
GCE   HRP/Au/CeO <sub>2</sub> -CS <sup>c</sup>	0.05-2.5	7.0	[33]
SPE   GS@CeO <sub>2</sub> -CuO	0.005-18.0	0.13	This work

<sup>a</sup> Limit of detection. <sup>b</sup> Glassy carbon electrode. <sup>c</sup> Chitosan.

### 3.6. Reproducibility, stability, selectivity, and real sample analysis

The reproducibility of the electrochemical sensor was measured at a  $\text{H}_2\text{O}_2$  concentration of 5.0 mM in 0.1 M PBS with the same SPE | GS@CeO<sub>2</sub>-CuO electrode. The current responses for five successive assays were recorded, and the relative standard deviation (*R.S.D.*) was 2.0%. Five different SPE | GS@CeO<sub>2</sub>-CuO electrodes prepared independently and the *R.S.D.* of electrode-to-electrode reproducibility was calculated to be 2.4%. Tests show a reliable reproducibility.

The SPE | GS@CeO<sub>2</sub>-CuO electrode was stored in a drying state at room temperature when not use. It was found that the current response kept about 92.2% of the initial value within 6 weeks. The result suggested that the modified electrode possesses a long-range stability.

The possible interferences that may effect the responses of the developed electrochemical sensor was investigated by i-t curve method (Fig. 9). The selectivity of the electrochemical sensor was tested by adding same concentration common co-existing electroactive compounds, such as glucose (Glu), ascorbic acid (AA), dopamine (DA) and uric acid (UA) in the presence of 1.0 mM  $\text{H}_2\text{O}_2$ . Results show that the current changes could be negligible, indicating a good selectivity. In essence, nano-sized GS, UA, AA molecules are all negatively charged, they will repel each other in the solution through electrostatic attraction [12]. Furthermore, the determination of  $\text{H}_2\text{O}_2$  on the SPE | GS@CeO<sub>2</sub>-CuO electrode at the working potential of -0.5 V is immune to glucose, DA, UA and AA.

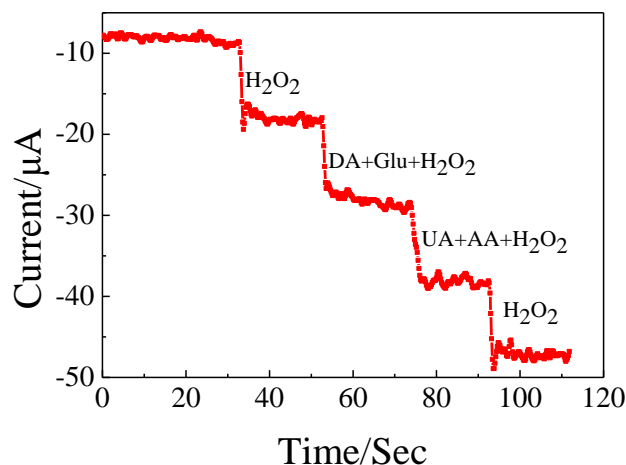


**Figure 9.** i-t curve of the SPE | GS@CeO<sub>2</sub>-CuO electrode at the effect of interfering substances during 1.0 mM  $\text{H}_2\text{O}_2$  detection.

For verifying the validity of the electrochemical sensor, the mentioned steps were used to determine  $\text{H}_2\text{O}_2$  in the real samples. 1.0 mL of real contact lens care solution sample was directly diluted into 100 mL with doubly distilled water. The  $\text{KMnO}_4$  titration method and recovery tests are applied to check the accuracy and reliability of this method. The  $\text{H}_2\text{O}_2$  contents and recoveries of added analyte are summarized in Table 2. Indicating the proposed method is a possible candidate to detect  $\text{H}_2\text{O}_2$  concentration in real samples.

**Table 2.** Determination results of H<sub>2</sub>O<sub>2</sub> in real samples (n=6, mM).

Samples	KMnO <sub>4</sub> titration	This method	Added	Found	R.S.D/%	Recovery/ %
1	5.20	5.19	5.0	10.07	4.3	97.6
2	5.15	5.12	5.0	10.08	4.1	99.2
3	5.18	5.12	5.0	10.15	3.5	100.6

#### 4. CONCLUSIONS

In conclusion, a novel and enhanced sensing platform for nonenzymatic H<sub>2</sub>O<sub>2</sub> based on facile synthesis of CuO doping into GS@CeO<sub>2</sub> nanocomposites sensitized SPE was fabricated. Due to being modified with hybrid nanomaterials, the proposed SPE | GS@CeO<sub>2</sub>-CuO electrode provides with high surface activity and could realize the nonenzymatic of H<sub>2</sub>O<sub>2</sub> as well as amplify the response currents. It also shows the advantages of wide LDR, low LOD and long-range stability compared with several typical nonenzymatic and enzymatic H<sub>2</sub>O<sub>2</sub> sensors. The proposed electrochemical sensor was successfully applied in the practical analytical. The excellent electrocatalytic performances enable the GS@CeO<sub>2</sub>-CuO based hybrid nanomaterials to determine other biological and chemical residues.

#### ACKNOWLEDGMENTS

The work was supported by the Key Project Foundation of Hunan Provincial Education Department (Nos. 14A025 and 16B1714) and the National Natural Science Foundation of China (No. 51308198).

#### References

1. V. Dharuman, C. Anjalidevi, P.N. Manikandan, H. Imran. *Anal. Methods*, 7 (2015) 3454-3460.
2. J. Narang, N. Chauhan, C.S. Pundir. *Analyst*, 136 (2011) 4460-4466.
3. N.M. Jia, B.Z. Huang, L.N. Chen, L. Tan, S.Z. Yao. *Sens. Actuators. B*, 195 (2014) 165-170.
4. S.N. Azizi, S. Ghasemi, A. Samadi-Maybodi, M. Ranjbar-Azad. *Sens. Actuators. B*, 216 (2015) 271-278.
5. L. Wang, M. Deng, G.H. Ding, S.H. Chen, F.G. Xu. *Electrochim. Acta*, 114 (2013) 416-423.
6. P.F. Pang, Z.M. Yang, S.X. Xiao, J.L. Xie, Y.L. Zhang, Y.T. Gao. *J. Electroanal. Chem.*, 727 (2014) 27-33.
7. L.X. Wang, X.J. Bo, J. Bai, L.D. Zhu, L.P. Guo. *Electroanalysis*, 22 (2010) 2536-2542.
8. H.F. Yue, X. Bu, M.H. Huang, J. Young, T. Raglione. *Int. J. of Pharm.*, 375 (2009) 33-40.
9. U. Pinkernell, S. Effkemann, U. Karst. *Anal. Chem.*, 69 (1997) 3623-3627.
10. W. Lei, A. Durkop, Z.H. Lin, M. Wu, O.S. Wolfbeis. *Microchim. Acta*, 143 (2003) 269-274.
11. N.V. Klassen, D. Marchington, H.C.E. McGowan. *Anal. Chem.*, 66 (1994) 2921-2925.
12. X. Yang, F.B. Xiao, H.W. Lin, F. Wu, D.Z. Chen, Z.Y. Wu. *Electrochim. Acta*, 109 (2013) 750-755.
13. X.R. Zhang, B.P. Qi, S.S. Zhang. *Anal. Lett*, 41 (2008) 3100-3112.
14. J.D. Qiu, S.G. Cui, R.P. Liang. *Microchim. Acta*, 171(2010) 333-339.
15. J.D. Qiu, S.G. Cui, M.Q. Deng, R.P. Liang. *J. Appl. Electrochem.*, 40 (2010) 1651-1657.
16. G.C. Zhao, Z.Z. Yin, L. Zhang, X.W. Wei. *Electrochem. Commun.*, 7 (2005) 256-260.

17. W. Liu, H.X. Zhang, B. Yang, Z.J. Li, L.C. Lei, X.W. Zhang. *J. Electroanal. Chem.*, 749 (2015) 62-67.
18. S.L. Yang, G. Li, G.F. Wang, J.H. Zhao, M.F. Hu, L.B. Qu. *Sens. Actuators, B*, 208 (2015) 593-599.
19. Y. Han, J.B. Zheng, S.Y. Dong. *Electrochim. Acta*, 90 (2013) 35-43.
20. L.B. Shi, X.H. Niu, T.T. Liu, H.L. Zhao, M.B. Lan. *Microchim. Acta*, 68 (2015) 358-364.
21. W. Zhao, H.C. Wang, X. Qin, X.S. Wang, Z.X. Zhao, Z.Y. Miao, L.L. Chen, M.M. Shan, Y.X. Fang, Q. Chen. *Talanta*, 80 (2009) 1029-1033.
22. S.H. Chen, R. Yuan, Y.Q. Chai, F.X. Hu. *Microchim. Acta*, 180 (2013) 15-32.
23. S.J. He, Z.G. Chen, Y.Y. Yu, L.J. Shi. *RSC Adv.*, 4 (2014) 45185-45190.
24. G.G. kumar, K.J. Babu, K.S. Nahm, Y.J. Hwang. *RSC Adv.*, 4 (2014) 7944-7951.
25. W.W. Wang, Y. Qiu, S.P. Zhang, J.W. Li, X.Q. Lu, X.H. Liu. *Chin. J. Anal. Chem.*, 42 (2014) 835-841.
26. P. Si, X.C. Dong, P. Chen, D.H. Kim. *J. Mater. Chem. B*, 1 (2013) 110-115.
27. S. Palanisamy, S.M. Chen, R. Sarawathi. *Sens. Actuators, B*, 166-167 (2012) 372-377.
28. D. Chirizzi, M.R. Guascito, E. Filippo, C. Malitesta, A. Tepore. *Talanta*, 147 (2016) 124-131.
29. Y.M. Sun, K. He, Z.F. Zhang, A.J. Zhou, H.W. Duan. *Biosens. Bioelectron.*, 68 (2015) 358-364.
30. X.H. Niu, H.L. Zhao, C. Chen, M.B. Lan. *Electrochim. Acta*, 65(2012) 97-103.
31. S.K. Vashist, J.H.T. Luong. *Carbon*, 84 (2015) 519-550.
32. S.K. Jha, C.N. Kumar, R.P. Raj, N.S. Jha, S. Mohan. *Electrochim. Acta*, 120 (2014) 308-313.
33. W. Zhang, G.M. Xie, S.F. Li, L.S. Lu, B. Liu. *Appl. Surf. Sci.*, 258 (2012) 8222-8227.
34. B.J. Wang, L.Q. Luo, Y.P. Ding, D.S. Zhao, Q.L. Zhang. *Colloids Surf., B.*, 97 (2012) 51-56.
35. C. Batchelor-McAuley, Y. Du, G.G. Wildgoose, R.G. Compton. *Sens. Actuators. B*, 135 (2008) 230-235.
36. X.M. Miao, R. Yuan, Y.Q. Chai, Y.T. Shi, Y.Y. Yuan. *J. Electroanal. Chem.*, 612 (2008) 157-163.
37. D. Chirizzi, M.R. Guascito, E. Filippo, C. Malitesta, A. Tepore. *Talanta*, 147 (2016) 124-131.
38. M.J. Song, S. W. Hwang, D. Whang, *Talanta*. 80 (2010) 1648-1652.
39. K.V. Ragavan, Navin K. Rastogi. *Sens. Actuators. B*, 229 (2016) 570-580.
40. T.T. Yang, J.K. Xu, L.M. Lu, X.F. Zhu, Y.S. Gao, H.K. Xing, Y.F. Yu, W.C. Ding, Z. Liu. *J. Electroanal. Chem.*, 761 (2016) 118-124.
41. X. Yang, F. Wu, D.Z. Chen, H.W. Lin. *Sens. Actuators. B*, 192 (2014) 529-535.
42. F. Wu, H.W. Lin, X. Yang, D.Z. Chen. *Int. J. Electrochem. Sci.*, 8 (2013) 7702-7712.
43. S. Jafari, F. Faridbod, P. Norouzi, A.S. Dezfouli, D. Ajloo, F. Mohammadipanah, M.R. Ganjali. *Anal. Chim. Acta* 895 (2015) 80-88.
44. G.W. He, X. Yang, Y.J. Hu, Y.J. Hu, F. Zhang. *Int. J. Electrochem. Sci.*, 9 (2014) 6962-6974.
45. Y.C. Li, Y.Y. Zhang, Y.M. Zhong, S.X. Li. *Appl. Surf. Sci.* 347 (2015) 428-434.
46. H.F. Liu, X.L. Chen, L.H. Huang, J. Wang, H.B. Pan. *Electroanalysis* 26 (2014) 556-564.